Fuel 274 (2020) 117798

Contents lists available at ScienceDirect

Fuel

journal homepage: www.elsevier.com/locate/fuel

Full Length Article

Impact of water salinity differential on a crude oil droplet constrained in a capillary: Pore-scale mechanisms

Lifei Yan, Hamed Aslannejad, S. Majid Hassanizadeh, Amir Raoof*

Department of Earth Sciences, Environmental Hydrogeology Group, Utrecht University, 3584 CB Utrecht, The Netherlands

ARTICLE INFO

Keywords:
Low-salinity effect
Oil droplet movement
Osmotic pressure
Contact angle change
Water diffusion
Water-in-oil emulsification

ABSTRACT

Low-salinity water flooding can be effectively used for enhanced oil recovery. Given the complex physical and chemical processes involved, several controlling mechanisms have been proposed to describe oil re-mobilization in the presence of water solution with low salinity. Osmosis and water-in-oil emulsification are among these mechanisms. However, our current knowledge about these processes is limited and their associated time scales are not well understood.

In this study, we have used 11 capillary tubes with an inner diameter of 800 μm to inject a sequence of low-salinity water, crude oil, and high-salinity water phases and to observe the evolution of the system. The monitoring was done for a period of 40 days. We used two setups, a CMOS camera and a confocal laser scanning microscopy, to capture dynamics of the oil droplet re-mobilization as well as the 2D/3D water–oil interfaces. Additionally, microscopic pore pressures were directly measured at both low and high-salinity water phases containing the oil droplet using two fiber-optic sensors.

We observed that in the water-wet capillaries the oil droplet moved a distance of about 524 μm. The contact angles at both low and high-salinity water interfaces with crude oil gradually decreased by 34.32° and 18.23°, respectively, during the first 15 days. We found that the pressure difference between high/low-salinity water phases reached a plateau with a maximum value of 1.65 kPa during a period of 24 days. Further, based on these changes and their time scales, we propose a hypothesis about emulsification and water diffusion through the oil phase.

1. Introduction

With the continuous exploitation of oil and gas fields, the application of enhanced oil recovery (EOR) has increased considerably in recent decades due to its potential to increase oil recovery by up to 60% of the original oil-in-place (OOIP) [1,2]. The three main techniques of EOR include gas injection, thermal injection, and chemical injection. For the application of the third technique, engineers consider low-salinity water flooding (LSWF) as a low-cost, effective, and more environmentally friendly technology. Compared with conventional and high-salinity water flooding, LSWF can improve oil recovery by about 5–38% based on the results from laboratory and field tests [3,4]. For instance, BP ran a field test of single-well chemical tracer tests (SWCTT) using low-salinity water injection in Alaska North Slope. It turned out that residual oil saturation substantially reduced and the corresponding oil recovery increased from 6 to 12% [5].

Although several lab tests and field applications proved the potential and efficiency of LSWF, the underlying mechanisms are still very controversial. Through the past 20 years, around 13 different responsible mechanisms have been proposed by researchers [6–8], including: (1) fine migration and mobilization [9], (2) wettability alteration [10], (3) reduced interfacial tension and increased pH effect [5,11,12], (4) multi-component ion exchange (MIE) [13], (5) double layer expansion [14], (6) emulsification and micro-dispersion [15], (7) osmotic pressure [16]. Various mechanisms responsible for the salinity effect have been comprehensively described in the above and other literature [17–19]. In the complicated brine/rock/crude oil system several mechanisms can act either individually or collectively towards oil re-mobilization. Wettability alteration is a widely accepted process. However, it is a follow-on phenomenon caused by multiple factors such as clay particles, pH, multi-ion exchange, pressure change, temperature change, and salt concentration. For instance, according to the theory of multi-ion exchange, absorbed divalent cations on the rock surface, such as Ca^{2+} and Mg^{2+}, can be replaced by the hydrogen ions as a result of local pH increase [12]. This exchange enhances the release of fines, and, therefore, decreases the rock permeability [20]. Furthermore, the

* Corresponding author.
E-mail address: A.Raoof@uu.nl (A. Raoof).

https://doi.org/10.1016/j.fuel.2020.117798
Received 16 December 2019; Received in revised form 3 March 2020; Accepted 4 April 2020
Available online 18 April 2020

pH increase leads to the reduction of oil–water interfacial tension and spontaneous water–oil emulsification [21]. At the same time, the saline water with lower ion strength enhances the electrostatic repulsion and double layer expansion, which increases the thickness of the water film located between oil and the rock surface. This process can alter the wettability toward a water-wet behaviour and may stabilize water–oil emulsion droplets [22,23]. The presence of several mechanisms shows that the low-salinity effect may not be explained using a single mechanism.

The fluid–fluid-solid interactions play a critical role in low-salinity effect, especially at the pore scale. Often, small influences induced by salinity concentration gradient and water–oil emulsions are ignored during low-salinity water flooding experiments in favour of other involved processes [24–26]. However, these processes can significantly change the rock wettability and oil movement in time period of days. Although some researchers [27–29] studied small changes of contact angle of water/oil under different salinities, the time scale of water–oil emulsion and osmotic gradient is not clear. Obviously, the contact time scale in reservoirs is much larger than an experimental period. For instance, the experimental period for pore-scale displacement and core flooding experiments is several minutes to hours, which may not be sufficiently large to observe the formation of water–oil emulsion and dynamic changes of the contact line.

Clearly, a real water–rock system is far more complicated than our system. The formation rocks contain various pore structures and complex minerals that provide numerous properties for capillary walls such as roughness, wettability, and electric charge [30,31]. These properties impact oil re-mobilization and water wetting actions on different scales [32,33]. Wettability of capillary walls, for example, can cause changes in oil/water displacement in micro-fluidics [34,35]. To provide consistent interpretations, we have used a simple setup under laboratory conditions by considering a uniform and clean solid surface to avoid the effect of other factors which otherwise can cause misinterpretation due to the unobserved mechanisms. In our study, to evaluate the contribution of osmosis and emulsification at the pore-scale, two aspects need attention: i) emulsion generation and water diffusion in the oil phase, ii) the effect of water–oil emulsion and chemical osmotic gradient on movement of the oil phase. In the following, we discuss these two aspects.

(i) Emulsion generation and water diffusion in the oil phase: in the application of low-salinity water flooding in a field, the water/oil emulsification and water micro-dispersion in oil are generally considered as the important contributors for boosting oil recovery [36,37]. In an environment with low ion strength, due to the double layer expansion, surfactants and clay particles can act as emulsifiers causing oil release and/or its detachment from the solid surfaces [38,39]. When the crude oil is in contact with water, the polar components in the crude oil, such as naphthenic acids, resins and asphaltenes, are adsorbed at the phase interface which could bond with water molecules and produce water-in-oil emulsions [40,41]. The polar portion, OH–, attracts water molecules through hydrogen bonding to form a hydrophilic head (water-like) toward the aqueous phase. The non-polar portion is a hydrophobic tail (oil-like) orientating toward the oil phase [42]. Consequently, a water-in-oil reverse micelle is formed (Fig. 1). A typical reverse micelle has a spherical shape with a size of ~ 50 Å and is made of about 100 surfactant molecules [43].

Miller (1988) discussed the water-in-oil spontaneous emulsification by diffusion in a ternary system consisting of water, a hydrocarbon, and surfactant [44]. Diffusion could lead to emulsification resulting in a region of local super-saturation for reaching an equilibrium state when aqueous and oleic phases with surfactant are brought into contact with each other. Emadi and Sohrabi (2013), using magnified images, observed that water micro-droplets formed in the crude the oil phase close to the interface [15]. They hypothesized that micro-dispersion of water, due to low-salinity water injection, was responsible for oil recovery. Evidences in the literature show that low-salinity water can accelerate

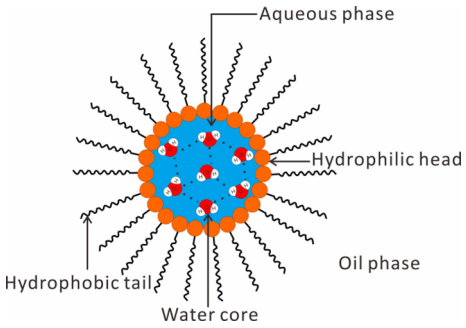

Fig. 1. Schematic diagram of a water-in-oil reverse micelle. The natural surfactant in crude oil typically has hydrophilic groups (their heads shown in orange colour) and hydrophobic groups (their tails shown in black colour), meaning it contains both a water-soluble and oil-soluble component. In the nonpolar phase, upon the introduction of water, the hydrophobic groups are attached to the water molecules by hydrogen–oxygen bond to reduce the free energy of the system. When the water concentration increases in the system, the surfactant molecules start to aggregate into nanoscopic water-in-oil reverse micelles so that the polar heads encapsulate the water core while the hydrophobic tails extend into the nonpolar phase. (For interpretation of the references to colour in this figure legend, the reader is referred to the web version of this article.)

the formation of water-in-oil emulsion and can increase water content of the oil [45,46]. Aldousary and Kovscek (2019) described that water hydrated ions can dissolve within the crude oil to reach to the equilibrium condition [39]. The solubility limit not only depends on crude oil type but also on brine salinity. As time passes, progressively more reverse micelles generate nearby interface to drive spontaneous emulsification [36,47].

Mokhtari and Ayatollahi (2019) determined that salinity can significantly affect the physical properties of the oil phase around the water–oil interface, e.g. pH, viscosity and density. In their experiments, they found a large number of emulsions after water and crude oil were in contact for a period of 45 days [48]. For the contact with lower salinity water (10 times diluted seawater), the dissolution of naphthenic acid in water and the formation of water-in-oil emulsion both increased, which caused a decrease of aqueous phase conductivity and pH by 22% and 6%, respectively. Meanwhile, microscopy imaging showed that water content in the oil phase was 3.95%, which was higher by 1.97% compared to its value for oil in contact with undiluted seawater. Additionally, the interface showed a rag-shape form due to the emulsion formation and asphaltene agglomerates, and a nearby increase of crude oil density.

To explain better the relationship between water content and brine salinity, we have plotted the relationship between brine salinity and water content in oil in Fig. 2 based on data from three studies listed in Table 1.

As shown in Fig. 2, in general, oil water-content decreases with the increase of salinity, however, may have a non-monotonic behaviour. Up to a salinity of about 6,600 ppm, water content decreases sharply from 7.34% to 0.66% with the increase of salinity. As the salinity increases up to about 40,000 ppm, water content increases to about 2% and then remains almost constant with a slight decrease. It is indeed known that, in a low-salinity water environment, when the salinity is less than a threshold value, there is a higher water content in the oil phase [25,48].

Alternatively, the interfacial tension (IFT) gradually increases with the increase of salinity [26,48,50–52]. Rostami (2019) performed micro-model experiments, and found the oil–water interface with two times diluted formation water had the largest number of asphaltene particles, and the interfacial tension was lowest compared to the results with higher water salinities [46]. When slightly increasing water salinity, e.g., adding a small amount of salt to pure water, the ions tend to interact with the polar components, and this causes IFT to decrease and

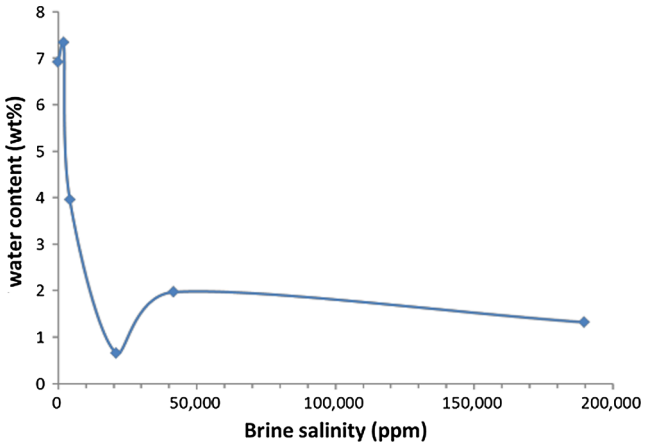

Fig. 2. The relationship between brine salinity and water content in oil. The graph is generated based on the data in Table 1.

read a minimum value at a given threshold salt concentration. At higher salt concentrations, more ions accumulate at the oil–water interface and the polar compounds in the oil phase become less ionized with lower tendency to move into the oil–water interface, remaining in the system with a high interfacial tension.

(ii) The effect of water–oil emulsion and chemical osmotic gradient on movement of the oil phase: considering a single pore occupied by a sequence of LSW, crude oil, and HSW, the water content within the oil phase near the LSW-oil interface is higher than, on the other side, near the HSW-oil because of emulsion formation [39]. The crude oil coming from the formation has reached the equilibrium with formation brine over extensive time and contains salt dissolved in the form of dispersed small water droplets [53]. The crude oil may even contain crystalline salt formed by pressure and temperature changes during production [54]. To explain the osmosis effect on oil re-mobilization, some researchers [55–57] suggest water transfer in oil from LSW to HSW contacts due to diffusion of water molecules and water-in-oil reverse micelle driven by the osmotic pressure generated by salinity difference of crude oil and LSW/HSW. However, some studies [15,45] hypothesized that the micro-dispersion of water into oil and its coalescence can cause swelling of the high-salinity water side, which leads to an increase in the pressure of the HSW side. The generated pressure can re-mobilize the trapped oil droplet. Therefore, the implication of water diffusion/dispersions in the oil phase is still not clear and the origin of pressure changes in the LSW-oil-HSW system are not well understood.

In order to explore the effect of water salinity, three questions should be addressed: i) how does the osmotic pressure affect oil re-mobilization in an LSW/Crude oil/HSW system? ii) What is the mechanism for generation of osmotic pressure and what is its magnitude? iii) How do the contact angles of LSW and HSW interfaces change due to oil re-mobilization over longer time periods?

In this study, to answer these questions, we prepared a number of sealed capillaries containing an LSW/Crude oil/HSW arrangement, which is similar to the situation shown in Fig. 3. Thus, we injected LSW, crude oil, and HSW in series into a capillary and monitored it for an extended period. We used a CCD camera, a confocal microscope, and pressure sensors to monitor continuously the oil droplet movement, changes in contact angles of the LSW/HSW interfaces and pressure in the LSW/HSW phases, respectively.

2. Formation of water-in-oil emulsions and water diffusion through the oil phase

2.1. Formation of water-in-oil micro-emulsion

Studies have shown that different salt concentrations lead to different water contents in the oil phase, due to the formation of water-in-oil micro-droplets, when water and crude oil are brought into contact with each other [39,45]. This process is a function of the water salinity. Fig. 3 illustrates the link between the formation of water-in-oil emulsion and salinity. There are two situations in the illustrations (Fig. 3a and 3b): one with the contacts of deionized water (DIW)/crude oil/HSW, and the other with the contacts of LSW/crude oil/HSW. In the case of the contact of DIW and crude oil, the situation is shown at the left side of Fig. 3a. As soon as oil meets deionized water, water molecules enter the oil phase and surface-active compounds (surfactants) near the oil–water interface start to combine with water molecules within oil and undergo a re-arrangement of their distribution in response to the present electrostatic attractions. The hydrophilic head is attracted toward a water molecule and non-polar portion points toward oil molecules [43]. The surfactants occupy surface sites, allowing more water to pass through the interface which may form water-in-oil emulsions nearby. The second situation is shown in the Fig. 3b. For water having the threshold salt concentration (the lowest IFT), in the left part of Fig. 3b, some water molecules combine with ions, such as Na^+, Cl^-, Ca^{2+}, SO_4^{2-}, to form an aqueous solution, which dominates the interface polarization effect. The ionic strength of LSW results in an increase in the adsorption of polar compounds at the interface. The accumulation of them leads to the lower interfacial tension. Meanwhile, the absorbed polar compounds start to take more surface sites instead of forming water-in-oil emulsions. Some generated reverse micelles may detach from the interface and pass through the oil phase [15,58]. Afterwards, the interface becomes a relatively complex system, including water–oil emulsions, water-encapsulated ions-oil emulsions, and dispersed anions and cations. For high-salinity environment, shown in the right part of Fig. 3a and 3b, the Debye length is much smaller, and this reduces the adhesion of polar components to the interface. Moreover, ions accumulate at the oil-brine interface and decrease the charge screening. Therefore, less oil–water emulsification occurs, and the interfacial tension increases comparing to the low-salinity ambient [25].

2.2. Water diffusion and reverse micelles transport in the oil phase

After the generation of water–oil emulsions, due to the difference of salinity between LSW and crude oil, that is equilibrated with formation water, reverse micelles as well as water molecules can diffuse through the oil phase by osmotic pressure. The diffusion of water molecules can be described by the Fick's equation [59]:

Table 1
The properties of different salinity brine and water content extracted from three literatures.

Brine type	Salinity (ppm)	Ion strength	Water content (wt%)	Data source
Formation water	189,682	3.674	1.32	2019-Mokhtari and Ayatollahi [48]
Sea water	41,659	0.832	1.97	
2 times diluted sea water	20,833	0.416	0.66	
10 times diluted sea water	4,162	0.0832	3.95	
Synthetic brine (NaCl and $CaCl_2$)	2,000	–	7.34	2014-Mahzari and Sohrabi [49]
Deionized water	0	0	6.92	2019-Aldousary and Kovscek [39]

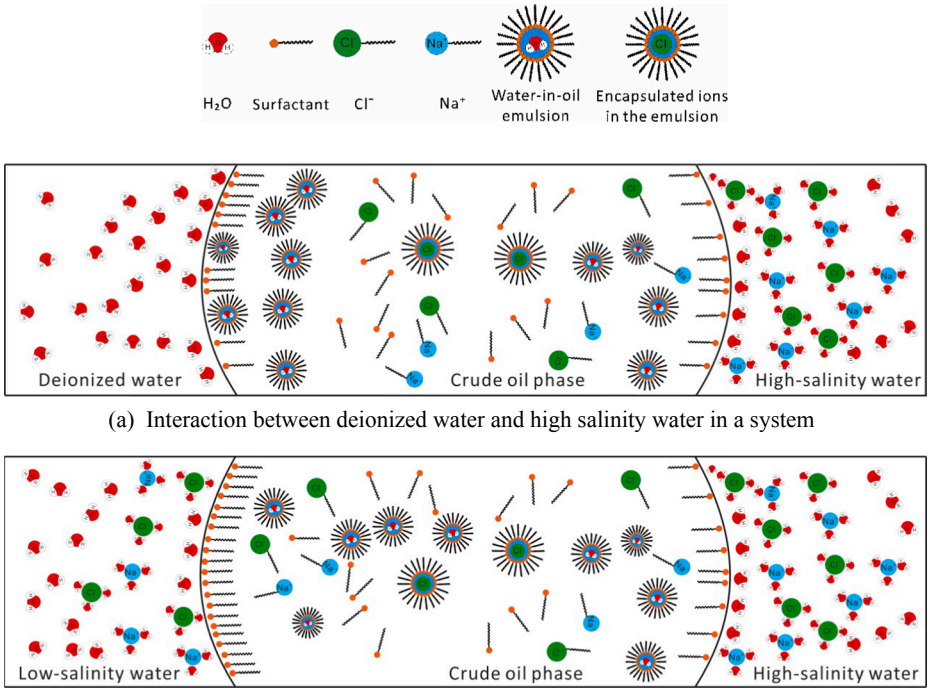

(a) Interaction between deionized water and high salinity water in a system

(b) Interaction between low-salinity water and high salinity water in a system

Fig. 3. The schematic diagram of interactions between crude oil and deionized water, low-salinity water, and high-salinity water phases. The crude oil phase is considered to have been in equilibrium with brine. Salt ions form complexes with positively and negatively charged organic compounds in oil. Water not only diffuses molecularly in oil but also exists as reverse micelles. When deionized water (shown in the left part of Fig. 3a) is brought into contact with equilibrated crude oil, the surfactants attract water molecules and aggregate them into reverse micelles, reducing the surface tension. With the increase in water concentration in oil, the formation of reverse micelles gets accelerated. In the case of LSW environment (the left part of Fig. 3b), the salt ions cause the polarization of interface, which can adsorb more polar compounds on the oil–water interface. The accumulation of polar compounds makes some reverse micelles away from interface. In the case of HSW environment, in the right part of plots 3a and 3b, the surface free energy increases due to the shorter Debye length. It results in the reduction of reverse micelle formation and makes surfactant stable around the interface.

$$\frac{\partial c}{\partial t} = D\frac{\partial^2 c}{\partial x^2} \tag{1}$$

where c is the concentration in the oil phase, t is time, D is the diffusion coefficient of ion in oil, and x is distance in the direction of diffusion. Aldousary and Kovscek (2019) pointed out that the diffusion coefficient of water molecules in oil is two orders of magnitude higher than that of hydrated ions [39]. It means that the diffusion of hydrated ions in crude oil may be negligible.

The diffusion coefficient can be approximated by the Stokes-Einstein equation [39,60].

$$D = \frac{k_B T}{6\pi\eta r} \tag{2}$$

where k_B is Boltzmann's constant, T is the absolute temperature, and r is the radius of the reverse micelle, η is the dynamic viscosity,.

The diffusion time scale is $t_d = L^2/D$, where L is the oil phase thickness. For typical situations, the dynamic viscosity of crude oil is 6.55×10^{-3} Pa·s, the reverse micelle radius is 50 Å, and the length of the oil phase is 1 cm, and the diffusion coefficient of a water reverse micelle would be around 6.56×10^{-11} m^2/s. So, the estimated time for a micelle to pass through the oil phase would be about 18 days.

Since the crude oil contains salty water initially dispersed in crude oil, we hypothesize that the chemical osmosis could occur when the crude oil is brought into contact with pure water or low-salinity water. If we assume the oil as an ideal semi permeable membrane, which only allows water molecules to pass through, the osmotic pressure can be described by Marine and Fritz (1981), based on van 't Hoff formula [61].

$$\Pi = \frac{RT}{V}\ln\left(\frac{a_1}{a_2}\right) \tag{3}$$

where Π is osmotic pressure, R is gas constant, V is partial molar volume of solvent, a_1 and a_2 are activity of water in low-salinity water and high-salinity water, respectively. For a non-ideal membrane, the reflection coefficient was introduced for the osmotic efficiency [62], which was defined as the ratio of observed osmotic pressure and the theoretical osmotic pressure at equilibrium.

$$\sigma = \left(\frac{\Delta P}{\Delta\Pi}\right)_{J_v=0} \tag{4}$$

where ΔP is the osmosis induced hydrostatic pressure in an ideal membrane, J_v is the net flux of solution across the membrane. Osmotic efficiency varies from 0 to 1 depending on membrane properties. Currently, the osmotic efficiency value for saline water in oil semi-membrane is not known so it is difficult to calculate an accurate value of osmotic pressure.

3. Experimental methods

3.1. Preparation of glass capillary and fluids property

We used 11 capillaries with an inner diameter of 800 ± 3 μm and length of 100 ± 0.20 mm made of borosilicate glass 3.3 (Hirschmann Laborgeräte GmbH &Co.). These capillaries were classified into two groups based on the capillary inner surface properties: water-wet (with a water contact angle < 90°) and oil-wet (with a water contact angle > 90°). The water-wet capillaries include No.1a-No.3b as well as No.6a and 6b, which have the original wettability of the glass (i.e., water wet). The oil-wet ones include No.4, No.5a and No.5b treated by salinization using trichloro- (1H,1H,2H,2H-perfluorooctyl) silane.

All capillaries were cleaned several times using deionized water and ethanol (≥96% (v/v) purchased from VWR International). After cleaning and air drying, three liquids were consecutively injected by a syringe pump (Harvard Apparatus 1 Pico Plus Elite Programmable Syringe Pump) into capillaries in the order of: i) low-salinity water, ii) crude oil, and iii) high-salinity water. The low-salinity water was a 10,000 ppm NaCl solution obtained by dissolving sodium chloride powder (purchased from Sigma-Aldrich) in deionized water. High-

Table 2
Properties of the crude oil, including Saturate, Aromatic, Resin and Asphaltene (SARA) components, density, and viscosity at 20°C.

Content	wt%
Saturates	45.4
Aromatics	42.19
Resin	12.28
Asphaltenes	0.13
Residual	0.99
Total Acid Number (TAN)	0.77 mg KOH/g
Density (g/cm^3)	0.9
Viscosity (mPa·s)	6.55

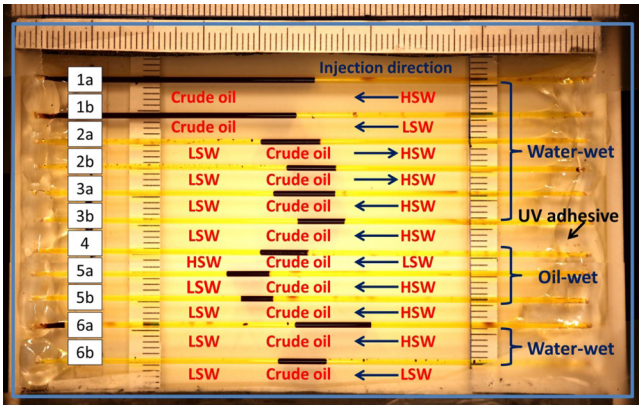

Fig. 4. The picture of six sets of capillaries with different processing situations. Each set has two capillaries as replicates (except No.4). The experiment number for each capillary is given on the left side of the figure. Types and injection directions of fluids (crude oil in black, brine in yellow) are marked with dark blue colour and arrows, respectively, under each capillary. The capillary inner surface wettability is provided in the right side of the figure. The top 6 and bottom 2 capillaries have the same water-wet wettability as borosilicate glass. No.4 to No.5b were treated with silane to become hydrophobic. We sealed all capillary ends using transparent UV adhesive (black arrow) and fixed them on a frame (blue rectangular). (For interpretation of the references to colour in this figure legend, the reader is referred to the web version of this article.)

salinity water was a 100,000 ppm NaCl solution. The properties of crude oil are listed in Table 2.

The capillaries were divided into 6 sets based on the sequence of fluid injections (determining the contact of glass capillary with different phases during the short injection period) and surface wettability (being water-wet or oil-wet). Each set had 2 capillaries as replicates (except experiment No.4 because the replicate capillary for No.4 was broken during the experiment). The injection velocity was 2 μL/min controlled by a syringe pump. The injection direction for each capillary is shown in Fig. 4 by blue colour arrows. Capillaries No.1a and No.1b were filled with half crude oil and half saline water as benchmark samples. Capillaries No.2a to No.3b were all filled with a sequence of LSW/Crude oil/HSW, however, as shown by blue arrows, filled from opposite ends of the capillary to consider the effect of possible wettability changes induced by injection sequence. No.4 through No.5b were filled in a similar order but capillaries were oil-wet. No.6a was firstly injected with a little amount of crude oil and then with LSW/Crude oil/HSW, which was also used to explore possible wettability effects due to the injection phase. To get insight into the behaviour of the system and collect complementary information, capillary No.6b was the reference capillary with LSW-crude oil-LSW (i.e., same water salinities on both sides of the oil phase). After preparation, the capillaries were sealed with Norland Optical Adhesive 81 (NOA81), which was cured by ultraviolet light into a hard polymer. Finally, the capillaries were fixed on a holding frame and placed on a board and monitored by a camera for 40 days at 21°C. During the observation period we carefully transported

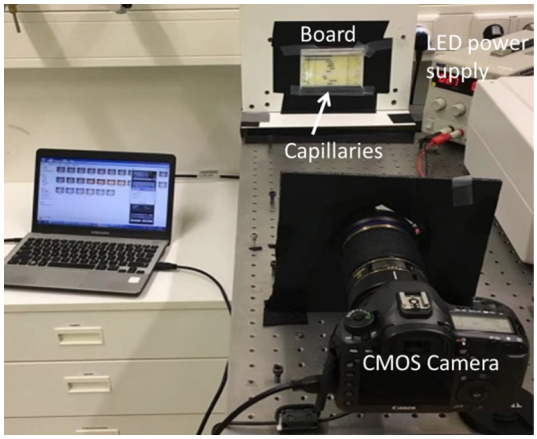

Fig. 5. A picture of CMOS camera set-up. The CMOS camera connected to a laptop to set the imaging frequency, and data acquisition. During the experiments, the setup was covered with a black box to avoid the effect of room light.

the plate with capillaries from the camera set-up to confocal set-up for taking 2D and 3D images of fluid interfaces in a time interval of two days.

3.2. Experimental set-up

3.2.1. CMOS camera set-up

In order to capture the oil droplet movement, we used a Canon 5D camera with EF 180 mm f/3.5L Macro USM lens shown in Fig. 5. The set-up consisted of a CMOS camera, a vertical board, an LED light source, and a laptop. All capillaries were put on a board in front of the LED light. We set the camera to take one photo per hour.

3.2.2. Confocal microscope set-up

In order to visualize the oil–water interfaces inside the capillary tubes, a confocal laser scanning microscope was used (Nikon A1 + Eclipse Ti inverted microscope with A1R confocal module). Confocal scanning microscopy uses imaging modality for optical sectioning of a capillary, which enables imaging of thin and small sections at high resolution. We used fluorescence confocal laser scanning microscope mode (CLSM) for 2D and 3D imaging reconstruction of water–oil interfaces. Specific fluorescent probes provided temporal and spatial colocalization of substances of interest.

High and low-salinity waters were dyed with fluorescein sodium salt (Sigma-Aldrich), which was used as a tracer for fluorescence recovery. The water part was visualized in green using a laser wavelength of 405 nm. The oil part in a capillary was seen in black. Optimization of imaging parameters yielded a distinction between water and oil resulting in a clear visualization of their interfaces. Images were captured using a 20x microscope objective and the view domain was 0.6×0.6 mm^2. In order to capture the entire interface of water and oil (in an XY plane), a bigger view domain would have been necessary. Since the inner diameter of the capillary tube is 800 μm, two images covering the entire diameter of the tube were taken and assembled into one image. To shorten the imaging time and limitation of the light to transfer large distances through the oil phase, given the cross-sectional symmetry of the capillary tube, half the capillary cross-section was imaged. A range of 2D optical sectioning was continuously conducted from the bottom to the middle of capillaries with multiple steps in the Z direction. After 2D image acquisition and combination, the 3D-image reconstruction of water was performed near the LSW-oil and HSW-oil interface, as shown in Fig. 6.

As shown in Fig. 6, dyed water and crude oil were shown as green and black colours, respectively. During the experiment period, the interfaces were imaged using confocal laser microscopy. Any change in

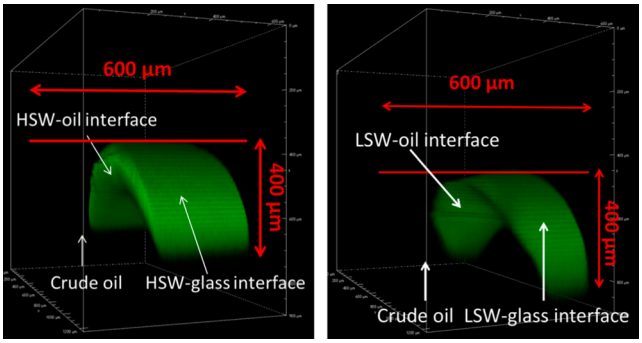

(a) 3D scanned part of capillary No.1a

(b) 3D scanned part of capillary No.1b

Fig. 6. Scanned parts of capillary No.1a and No.1b around the interfaces. Scan area was 600 μm× 400 μm× 800 μm. The glass edge is shown in red lines. The oil phase is on the left part of scan area and is black. Water phase is on the right part of scan are and is green. The interface between oil and water is the cavity as shown by white arrows. The top curved part is the interface between brine and glass tubes. Only half of the interfaces are scanned. Due to the penetration limitation of the laser, closer to the middle of the tube less light could penetrate and interface is therefore less visible. However, as shown in Fig. 6, the interfaces in the half of tube could be imaged accurately. (For interpretation of the references to colour in this figure legend, the reader is referred to the web version of this article.)

interfaces were monitored. We took 2D and 3D images of all water–oil interfaces every two to three days, so the dynamic changes of contact angle and contact line could be monitored with 2D scanning slices and 3D reconstruction.

3.2.3. Pressure monitoring set-up

To observe the pressure changes in the capillaries, two fiber-optic micro-transducers were planted in the LSW and HSW ends of a capillary, as shown in Fig. 7. The pressure sensor has a cylindrical cavity with a diameter of 260 μm at the front, connecting with a sensor module through a ϕ160 μm optic fiber. The measurement ranges from 40 Pa up to 40 kPa with a resolution of 40 Pa. The accuracy is 0.6% of full range. The details of pressure sensors and monitoring set-up can be found in literature references [63] and [64]. With this set-up, the pressures of LSW and HSW could be recorded every 8 min for 40 days.

Our experimental observations and data analysis made it possible to study three main issues. methods, oil droplet movement, contact angle changes, and pressure changes in the capillaries.

4. Results and discussion

4.1. Oil droplet movement

In order to quantify the oil phase movement, we processed the camera images using ImageJ software. The main steps of image processing are shown in the Supplementary material: cropping oil parts of images, making binary images, subtracting the oil areas with wand tool, then measuring the length difference of the front and end of oil droplets

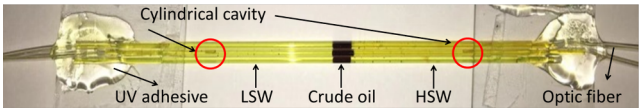

Fig. 7. Two fiber optic micro-transducers used as pressure sensors in the capillary. Three capillaries were prepared with LSW, crude oil, and HSW using the same method as in the section 3.1. Two pressure sensors were plugged into LSW and HSW separately. The positions of transducer heads are shown by red circles. (For interpretation of the references to colour in this figure legend, the reader is referred to the web version of this article.)

from the beginning to the end of experiment.

The amount and direction of displacement of oil droplets within 40 days are shown in Fig. 8. The positive value shows oil movement toward the LSW side, while the negative value is for the reverse direction. In capillary No.1a and No.1b with half-crude oil and half HSW or LSW, respectively, the oil phase moved towards the aqueous phase because of the emulsification of water into oil [15,53]. The measurement error is ± 20 μm.

Fig. 8 shows oil displacement for nine capillaries (based on experimental conditions shown as No.2a to No.6b). We can see that the oil droplets in water-wet capillaries, No.2a to No.3a, as well as in oil-wet capillary, No.5a, moved from the HSW side towards the LSW side. The maximum the oil phase movements were around 524 μm and 664 μm in water-wet capillaries and oil-wet capillaries, respectively. However, the oil droplets showed an opposite movement of oil droplet in the capillaries No.3b, No.4 and No.6a. For the capillaries No.3b and No.4, we observed that the menisci between oil droplet and LSW/HSW became highly irregular. These irregular menisci occurred at the beginning of experiment when three fluids were injected into one capillary and was not gradually generating during the experimental period. This is because, due to different viscosities of oil and water, during the injection phase obtaining a perfect water–oil meniscus for all capillaries was difficult. Such interface irregularities are reported in literature which also made uncertainty for pressure distribution over the menisci compared to interfaces with clear and regular shapes [65,66]. For capillary No.6a, we injected a small volume of crude oil prior to the injection of LSW. Although the possible wettability effects, due to the injection phase can be decreased with this method, meanwhile crude oil could change wettability by leaving behind a thin film of oil along the capillary [67]. Such oil films can affect displacement of the oil droplet [68]. The reference capillary No.6b had LSW on both sides of the oil phase contained the same salinity, where no significant movement of the oil phase was observed. The nine capillary experiments show that oil droplet displacement is mostly affected by difference in salinity of water on the two sides of the oil.

Based on the obtained images, we measured the average displacement as well as speed of movement for oil–water meniscus over time (Fig. 9a-b). In order to fully present meniscus movement over 40 days, we considered averaging the movement of contact point among water, oil and glass, and the movement of oil-LSW and oil-HSW menisci for each oil droplet. Using these data, the speed of meniscus movement was also calculated, which indicated presence of 3 stages: i) interface curvature change, ii) significant movement of the oil phase, and iii) slow movement of the oil phase (Fig. 9). The first stage includes changes of interface curvature mainly controlled by the wettability of the solid surface and the time needed for the meniscus to reach the equilibrium. For example, in the water-wet capillaries, the meniscus curvature increased compared to those in the oil-wet capillaries while no large bulk-phase movements were observed in this stage. The contact angle with the low-salinity water dramatically decreased within the first 10 days. More details about contact angle changes will be discussed in Section 4.2. The second stage occurred during 14–22 days after start of experiments. In this stage, most of capillaries had obvious meniscus movements (averaged values > 100 μm), where the oil droplets started to move. The time scale for this stage is comparable with the time scale for water diffusion through the oil phase (described in Section 2.2) which has been reported by other studies as well [39]. The magnitude of meniscus movement in this period mainly represents the bulk oil movement rather than change of interface curvatures. During this stage, which includes transfer of water from the LSW side towards the HSW side, the pressure in HSW side started to increase so that the pressure difference between LSW and HSW sides slowly reached to a maximum value [15,57]. Next, during the third stage, the oil phase showed movement with lower speed, compared to the second stage, as the pressure differences between the two ends started to diminish. Therefore, stage three includes the gradual decrease of the established pressure difference over time which is discussed in Section 4.3.

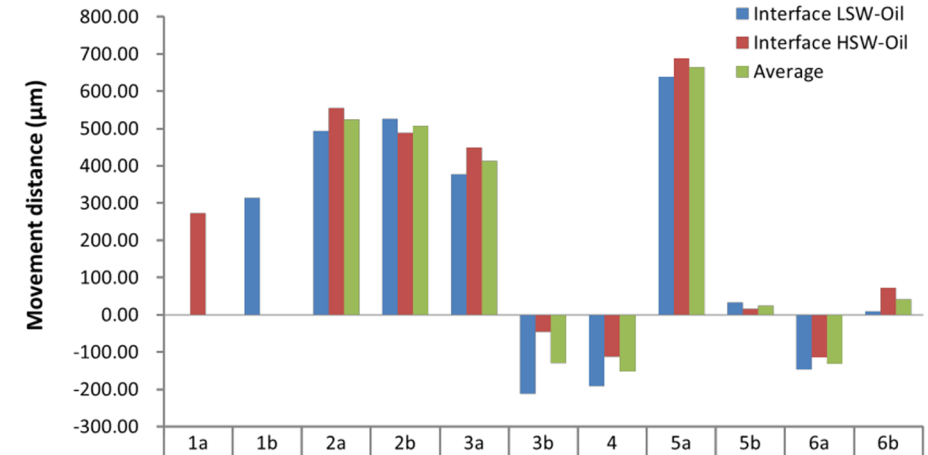

	1a	1b	2a	2b	3a	3b	4	5a	5b	6a	6b
Interface LSW-Oil		313.61	492.80	525.72	376.89	-212.62	-192.04	639.23	32.93	-147.41	9.70
Interface HSW-Oil	272.13		554.87	488.10	449.59	-46.55	-113.17	688.61	15.17	-114.26	73.05
Average			523.83	506.91	413.24	-129.58	-152.61	663.92	24.05	-130.84	41.38

Fig. 8. The movement of oil droplet. The positive values indicate that the oil droplet moved from the side with HSW to the side with LSW. The negative value means oil moved in the opposite direction. The values for capillaries No.1a and 1b mean that the interface between oil and brine moved toward the water side. The movement of oil droplet is shown using three numbers in blue, red, and green, respectively, showing the amount of movement based on the LSW-oil meniscus, HSW-oil meniscus, and average value. (For interpretation of the references to colour in this figure legend, the reader is referred to the web version of this article.)

4.2. Contact angle measurement

Contact angles of brine-oil-glass in all capillaries were captured and measured using confocal microscope. Taking capillary No.2a as an example, the changes in contact angle of LSW-oil and HSW-oil interfaces are shown in Fig. 10. The measurement error is ± 1°.

In Fig. 11, all curves in the first 10 days sharply dropped, meaning that both LSW and HSW can increase water wettability of the surface. The alteration generally takes 10–14 days based on the trend of contact angle changes. The contact angle on the LSW side has the most reduction with the maximum value of about 34° in capillary No.2a showing 16% change of the contact angle. The changes of contact angles on HSW side are around 18° providing a 5% change. After about 14 days, the changes on LSW side show slow reduction, but those on HSW side become larger or stops changing. These behaviours can be caused by the oil movement as at the HSW side the interface passes a region which was previously in contact with oil (i.e., the original location of the oil phase) and became slightly oil wet (e.g., graphs 2a and 3a in the right plot of Fig. 11 showing the contact angle of HSW side sharply increased by even up to around 60°). Moreover, from Fig. 11(a), we can conclude that the water-wet capillaries have larger contact angle changes compared to the oil-wet capillaries. In the first 14 days, the water-wet capillaries had an average reduction of about 17°, while the oil-wet capillaries had an average reduction of only 4°.

4.3. Pressure changes in a capillary

Using the pore-scale pressure monitoring set-up, the pressure changes were continuously monitored in LSW and HSW phases in capillary No.2a using two micro pressure sensors. The sensors were set to an initial value of zero and set to record a value every eight minutes. Results of pressure difference with two values per day are shown in Fig. 12 together with the measured LSW-side contact angle.

According to the measurements of meniscus movement, we can explain the pressure difference according to the three stages (marked with numbers in the top section of Fig. 12) as: i) gradual increase of pressure difference, ii) pressure difference reaches a plateau, and iii) decay of pressure difference. In stage one, the curvatures changes of LSW-oil and HSW-oil menisci induce a growth of pressure in LSW and HSW phases. During the 6th to 12th day, pressure difference gradually reached a plateau with the maximum value 1,650 Pa, which caused by the processes of dissolution and emulsion formation of water into the oil phase [44]. The LSW-side lost more water than the HSW-side so that the pressure drop in LSW-side was larger which can explain the

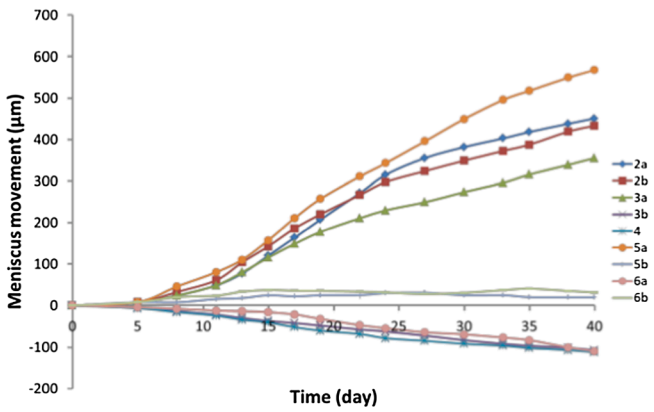

(a) Meniscus movement

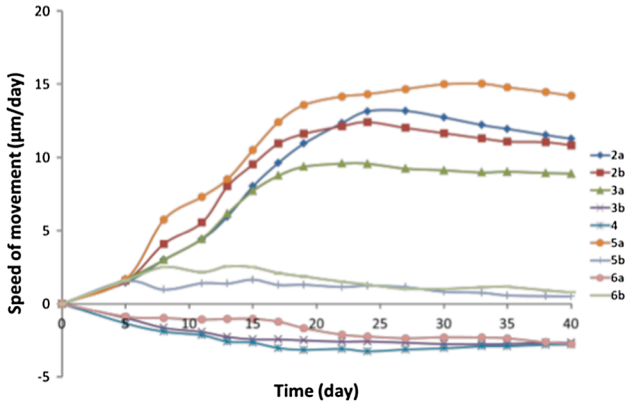

(b) Speed of meniscus movement

Fig. 9. The movement of meniscus over time (a) and its associated speed (b) belonging to capillaries No.2a to No.6b for a period of 40 days. There are 16 average values of meniscus movement for each capillary (i.e., we selected one image per 2–3 days). The measurement was obtained after processing the images using the ImageJ software. In Fig. 9a, the positive values indicate a movement of oil droplet from the side with HSW to the side with LSW. The negative values indicate oil movement in the opposite direction. In Fig. 9b, the speed of movement was calculated as $\frac{dx}{dt}$, where dx was the movement difference between two measurement points, and dt was the associated elapsed time.

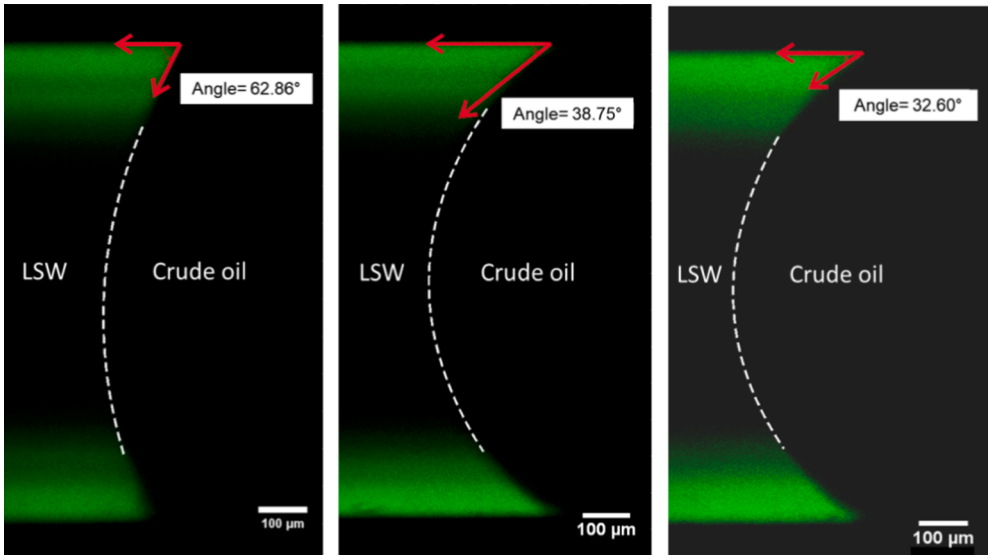

(a) After 1 day (b) After 15 days (c) After 40 days

Fig. 10. 2D-images of contact angle changes of LSW side in the capillary No.2a. The contact angles after 1 day, 15 days, and 40 days are measured and shown in plots (a), (b), and (c), respectively. As discussed in Section 3, the confocal microscope scanned half of the capillary. Scanning area includes several different layers in depth. We have chosen the layer that is closest to middle of the capillary for capturing the most precise contact angle. In this case, due to the penetration limitation of the laser, the middle part of interfaces missed from the observation. The white dashed lines in pictures illustrate the missing part of interfaces. The green parts represent the LSW phase (showed on the left of the white lines). The section to the right of the white lines indicates the crude the oil phase. (For interpretation of the references to colour in this figure legend, the reader is referred to the web version of this article.)

movement of oil droplets in the capillary No.1a and No.1b. Both the oil phases invaded into brine phase [69,70]. In stage two, a relative stable pressure difference is established between HSW and LSW sides with a value of around 1,400 Pa. As observed by other studies [70], water diffusion due to osmotic pressure between LSW and crude oil as well as between HSW and crude oil causes transfer of water along the capillary. In our works, the osmosis and water diffusion possibly cause the pressure difference. Moreover, the period of forming a plateau, from the 12th to 22th day, agree with the second stage of meniscus movement. The meniscus at this stage showed significant movement and some of them showed a faster movement than those in the third stage. In the third stage, from 23th to the 40th day, the pressure difference decays to get back almost to a zero value. This can be due to reaching equilibrium between salt concentrations in LSW and HSW sides after water diffusion from LSW side to HSW side. Based on Fig. 12, within the first 10 days, the contact angle dramatically decreased. Afterwards, the contact angle maintained a value of around 38° for about 15 days. From the 24th day onwards, the contact angle slowly dropped about 6°, which is overall consistent with the result from pressure change measurements.

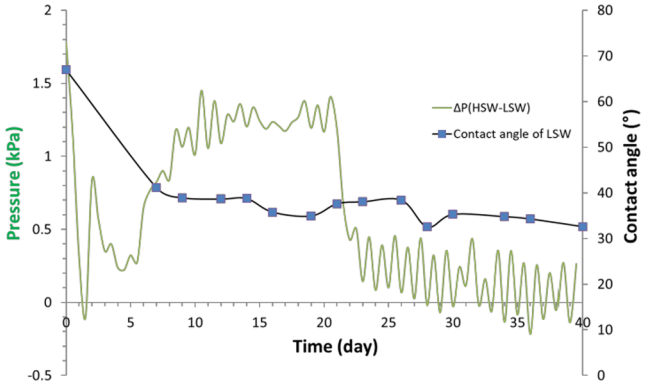

Fig. 12. Graphs of monitored pressure difference in HSW and LSW phase in capillary No.2a. The green curve shows the pressure difference. The fluctuations in the curve may come from the atmospheric pressure variation around sensors because of slight fluctuations of room temperature. The contact angle of LSW in capillary No.2a is also shown as a black curve for comparison with the tendency of pressure. (For interpretation of the references to colour in this figure legend, the reader is referred to the web version of this article.)

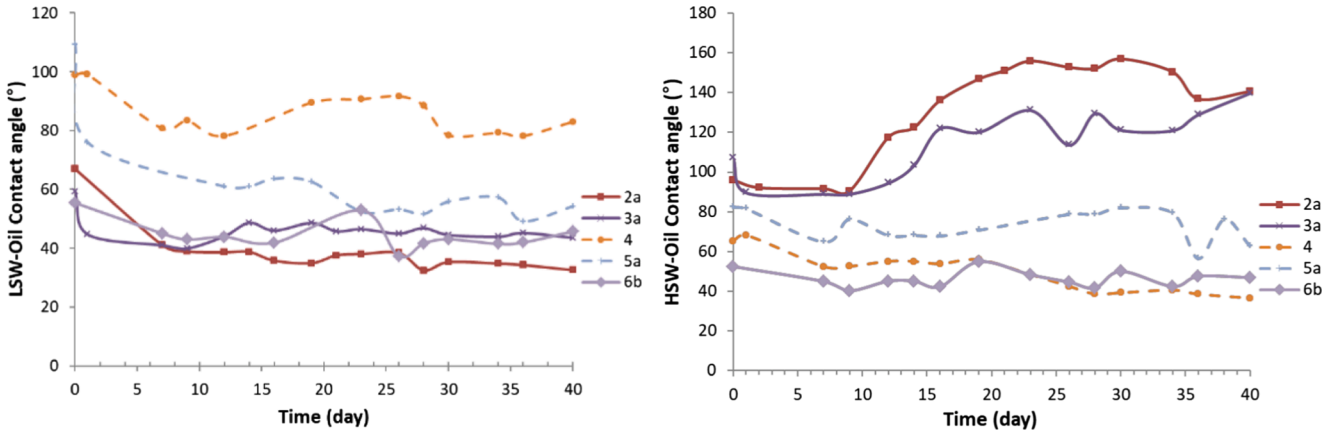

(a) contact angle of LS Wside (b) contact angle of HS Wside

Fig. 11. Change of contact angles in LSW sides (shown on the left plot) and HSW sides (shown on the right plot). There are 16 points for each curve. Solid curves represent the water-wet capillaries. Dashed ones are for the oil-wet capillaries.

4.4. Future research

This study introduced methods and results for monitoring oil droplet movement and measuring pressure change in a capillary. We observed the movement of oil droplets and contact angle changes using a CMOS camera set-up and a confocal microscope, respectively. Besides, the pressures in LSW and HSW phases for a long-time period (40 days) were detected.

Based on our measurements and mechanisms reported in the literature, we could explain the dynamic of the system using spontaneous emulsification and osmosis processes. The relative theories have been expressed by many researchers [15,39,44,70]. Yet, the very complex and coupled chemical and physical interactions between brine and crude oil requires future work to characterize the system fully. Future research is needed to i) observe and characterise the emulsification process especially adjacent to water–oil interfaces, ii) obtain more data on pressure changes in the LSW/Crude oil/HSW system. A dynamic measurement and characterization of the chemical evolution of different phases of the system would be ideal to confirm the presence of proposed mechanisms, which is, however, very challenging due to the small volumes of fluid phases used in capillary experiments.

5. Conclusion

In the complex subsurface fluid-rock settings several factors such as fluid properties, multiple factors can influence the re-mobilization of trapped oil. Examples are rock surface roughness, mineral heterogeneity, oil composition, pore and throat size and shape. Our study provides insight on the effect of osmosis and emulsification on the oil mobilization and water transport in oil at the scale of pore-scale capillary. Our experiments are conducted under the relatively ideal conditions such as synthetic brine, and a smooth, clean and mineral homogeneous solid surface. We have used two different monitoring setups to enable us to dynamically capture both the movement of oil droplet and the changes in 2D/3D contact interfaces at the water–oil-glass contact. The effect of salinity change on the confined crude oil droplet is explained by two mechanisms: emulsification and water diffusion through the oil phase. In particular, this study showed that:

i. Oil droplets can be re-mobilized by water diffusion in crude oil. We could observe and measure the resulting oil movement.
ii. Based on the contact angle measurement of low/high-salinity water, we can confirm that LSW and HSW both have the potential of driving the capillary containment surface towards water-wet behaviour, while LSW was more effective to make hydrophilic surfaces water-wet, compared to its impact on the hydrophobic surface.
iii. Pressure change of pore water with low and high salinity is directly monitored, and its tendency is consistent with the change of contact angle and oil movement. The measured pressures, additionally, validated the water diffusion and osmosis effect mechanisms.
iv. Based on time scales and the dominant processes, we proposed three stages for the changes in contact angle and pressure.

CRediT authorship contribution statement

Lifei Yan: Conceptualization, Methodology, Writing - original draft, Investigation, Formal analysis. **Hamed Aslannejad:** Data curation, Visualization. **S. Majid Hassanizadeh:** Conceptualization, Writing - review & editing. **Amir Raoof:** Supervision, Writing - review & editing.

Declaration of Competing Interest

The authors declare that they have no known competing financial interests or personal relationships that could have appeared to influence the work reported in this paper.

Acknowledgment

The authors acknowledge the support by China Scholarship Council (No. 201609120013). The authors gratefully acknowledge professor Ruud Schotting, Enno de Vries, and Luwen Zhuang for their helpful ideas, and thanks to Ioannis Zarikos and Mahin Baghery for technical support. Many thanks to the reviewers for giving the helpful comments.

Appendix A. Supplementary data

Supplementary data to this article can be found online at https://doi.org/10.1016/j.fuel.2020.117798.

References

[1] J. Sheng, Enhanced oil recovery field case studies. Gulf Professional Publishing, 2013.
[2] Z. Bachari, A. A. Isari, H. Mahmoudi, S. Moradi, and E. H. Mahvelati, "Application of Natural Surfactants for Enhanced Oil Recovery–Critical Review," in IOP Conference Series: Earth and Environmental Science, 2019, vol. 221, no. 1, p. 012039: IOP Publishing.
[3] S. Kokal and A. Al-Kaabi, "Enhanced oil recovery: challenges & opportunities," World Petroleum Council: Official Publication, vol. 64, 2010.
[4] D. A. Wood and B. Yuan, "Low-Salinity Water Flooding: from Novel to Mature Technology," in Formation Damage During Improved Oil Recovery: Elsevier, 2018, pp. 21-67.
[5] P. McGuire, J. Chatham, F. Paskvan, D. Sommer, and F. Carini, "Low salinity oil recovery: An exciting new EOR opportunity for Alaska's North Slope," in SPE western regional meeting, 2005: Society of Petroleum Engineers.
[6] Wang L, Fu X. Data-driven analyses of low salinity water flooding in sandstones. Fuel 2018;234:674–86.
[7] Fattahi A. Low Salinity Waterflooding in sandstone-A review. Int. J Petrol Geosci Eng 2014;2(4):315–41.
[8] Al-Shalabi EW, Sepehrnoori K. A comprehensive review of low salinity/engineered water injections and their applications in sandstone and carbonate rocks. J Petrol Sci Eng 2016;139:137–61.
[9] Tang G, Morrow NR. Salinity, temperature, oil composition, and oil recovery by waterflooding. SPE Reservoir Eng 1997;12(04):269–76.
[10] Buckley J, Liu Y, Monsterleet S. Mechanisms of wetting alteration by crude oils. SPE J 1998;3(01):54–61.
[11] Y. Zhang and N. R. Morrow, "Comparison of secondary and tertiary recovery with change in injection brine composition for crude-oil/sandstone combinations," in SPE/DOE symposium on improved oil recovery, 2006: Society of Petroleum Engineers.
[12] T. Austad, "Water-based EOR in carbonates and sandstones: New chemical understanding of the EOR potential using "Smart Water"," in Enhanced oil recovery Field case studies: Elsevier, 2013, pp. 301-335.
[13] A. Lager, K. J. Webb, C. Black, M. Singleton, and K. S. Sorbie, "Low salinity oil recovery-an experimental investigation1," Petrophysics, vol. 49, no. 01, 2008.
[14] D. J. Ligthelm, J. Gronsveld, J. Hofman, N. Brussee, F. Marcelis, and H. van der Linde, "Novel Waterflooding Strategy By Manipulation Of Injection Brine Composition," in EUROPEC/EAGE conference and exhibition, 2009: Society of Petroleum Engineers.
[15] A. Emadi and M. Sohrabi, "Visual investigation of oil recovery by low salinity water injection: formation of water micro-dispersions and wettability alteration," in SPE annual technical conference and exhibition, 2013, vol. 30: Society of Petroleum Engineers.
[16] K. Sandengen and O. Arntzen, "Osmosis during low salinity water flooding," in IOR 2013-17th European Symposium on Improved Oil Recovery, 2013.
[17] Zhang L, et al. Experimental investigation of low-salinity water flooding in a low-permeability oil reservoir. Energy Fuels 2018;32(3):3108–18.
[18] Awolayo AN, Sarma HK, Nghiem LX. Brine-dependent recovery processes in carbonate and sandstone petroleum reservoirs: review of laboratory-field studies, interfacial mechanisms and modeling attempts. Energies 2018;11(11):3020.
[19] Derkani MH, Fletcher AJ, Abdallah W, Sauerer B, Anderson J, Zhang ZJ. Low salinity waterflooding in carbonate reservoirs: review of interfacial mechanisms. Colloids and Interfaces 2018;2(2):20.
[20] Valdya R, Fogler H. Fines migration and formation damage: influence of pH and ion exchange. SPE Prod Eng 1992;7(04):325–30.
[21] J. Sheng, Modern chemical enhanced oil recovery: theory and practice. Gulf Professional Publishing, 2010.
[22] Khilar KC, Fogler HS. The existence of a critical salt concentration for particle release. J Colloid Interface Sci 1984;101(1):214–24.
[23] Nasralla RA, Nasr-El-Din HA. Double-layer expansion: is it a primary mechanism of improved oil recovery by low-salinity waterflooding? SPE Reservoir Eval Eng 2014;17(01):49–59.
[24] Bartels W-B, Mahani H, Berg S, Hassanizadeh S. Literature review of low salinity waterflooding from a length and time scale perspective. Fuel 2019;236:338–53.
[25] K. H. Chakravarty, P. L. Fosbøl, and K. Thomsen, "Brine crude oil interactions at the Oil-Water Interface," in SPE Asia Pacific Enhanced Oil Recovery Conference, 2015: Society of Petroleum Engineers.

[26] Wei B, et al. Influence of Individual Ions on Oil/Brine/Rock Interfacial Interactions and Oil-Water Flow Behaviors in Porous Media. Energy Fuels 2017;31(11):12035–45.
[27] Mahani H, Keya AL, Berg S, Bartels W-B, Nasralla R, Rossen WR. Insights into the mechanism of wettability alteration by low-salinity flooding (LSF) in carbonates. Energy Fuels 2015;29(3):1352–67.
[28] Mahani H, Berg S, Ilic D, Bartels W-B, Joekar-Niasar V. Kinetics of low-salinity-flooding effect. SPE J 2015;20(01):8–20.
[29] W.-B. Bartels, H. Mahani, S. Berg, R. Menezes, J. van der Hoeven, and A. Fadili, "Low salinity flooding (LSF) in sandstones at pore scale: micro-model development and investigation," in SPE Annual Technical Conference and Exhibition, 2016: Society of Petroleum Engineers.
[30] Nelson PH. Pore-throat sizes in sandstones, tight sandstones, and shales. AAPG Bull 2009;93(3):329–40.
[31] Brady PV, Krumhansl JL. A surface complexation model of oil–brine–sandstone interfaces at 100 C: Low salinity waterflooding. J Petrol Sci Eng 2012;81:171–6.
[32] Bottiglione F, Carbone G, Persson BN. Fluid contact angle on solid surfaces: role of multiscale surface roughness. J Chem Phys 2015;143(13):134705.
[33] Tokunaga TK, Wan J. Water film flow along fracture surfaces of porous rock. Water Resour Res 1997;33(6):1287–95.
[34] Tanino Y, Zacarias-Hernandez X, Christensen M. Oil/water displacement in microfluidic packed beds under weakly water-wetting conditions: competition between precursor film flow and piston-like displacement. Exp Fluids 2018;59(2):35.
[35] Songok J, Toivakka M. Enhancing capillary-driven flow for paper-based microfluidic channels. ACS Appl Mater Interfaces 2016;8(44):30523–30.
[36] Evdokimov IN, Fesan AA, Kronin AM, Losev AP. Common Features of "Rag" Layers in Water-in-Crude Oil Emulsions with Different Stability. Possible Presence of Spontaneous Emulsification. J Dispersion Sci Technol 2016;37(11):1535–43.
[37] Riehm DA, Rokke DJ, Paul PG, Lee HS, Vizanko BS, McCormick AV. Dispersion of oil into water using lecithin-Tween 80 blends: The role of spontaneous emulsification. J Colloid Interface Sci 2017;487:52–9.
[38] Song W, Kovscek AR. Spontaneous clay Pickering emulsification. Colloids Surf, A 2019;577:158–66.
[39] Aldousary S, Kovscek AR. The diffusion of water through oil contributes to spontaneous emulsification during low salinity waterflooding. J Petrol Sci Eng 2019;179:606–14.
[40] Speight JG. The chemistry and technology of petroleum. CRC Press; 2014.
[41] I. G. Sørbø, "Polar Components in Crude Oils and Their Correlation to Physiochemical Properties," The University of Bergen, 2016.
[42] Malik MA, Wani MY, Hashim MA. Microemulsion method: A novel route to synthesize organic and inorganic nanomaterials: 1st Nano Update. Arabian J Chem 2012;5(4):397–417.
[43] Goyal P, Aswal V. Micellar structure and inter-micelle interactions in micellar solutions: results of small angle neutron scattering studies. Curr Sci Bangalore 2001;80(8):972–9.
[44] Miller CA. Spontaneous emulsification produced by diffusion—a review. Colloids Surf 1988;29(1):89–102.
[45] P. Mahzari and M. Sohrabi, "Crude oil/brine interactions and spontaneous formation of micro-dispersions in low salinity water injection," in SPE improved oil recovery symposium, 2014: Society of Petroleum Engineers.
[46] P. Rostami, M. F. Mehraban, M. Sharifi, M. Dejam, and S. Ayatollahi, "Effect of water salinity on oil/brine interfacial behaviour during low salinity waterflooding: A mechanistic study," Petroleum, 2019.
[47] Umar AA, Saaid IBM, Sulaimon AA, Pilus RBM. A review of petroleum emulsions and recent progress on water-in-crude oil emulsions stabilized by natural surfactants and solids. J Petrol Sci Eng 2018;165:673–90.
[48] Mokhtari R, Ayatollahi S. Dissociation of polar oil components in low salinity water and its impact on crude oil–brine interfacial interactions and physical properties. Pet Sci 2019;16(2):328–43.
[49] Mahzari P, Sohrabi M, Cooke AJ, Carnegie A. Direct pore-scale visualization of interactions between different crude oils and low salinity brine. J Petrol Sci Eng 2018;166:73–84.
[50] Hua Z, Li M, Ni X, Wang H, Yang Z, Lin M. Effect of injection brine composition on wettability and oil recovery in sandstone reservoirs. Fuel 2016;182:687–95.
[51] Ayirala SC, Al-Yousef AA, Li Z, Xu Z. Water Ion Interactions at Crude-Oil/Water Interface and Their Implications for Smart Waterflooding in Carbonates. SPE J 2018.
[52] Binks BP, Horozov TS. Colloidal particles at liquid interfaces. Cambridge University Press; 2006.
[53] Du Y, Xu K, Mejia L, Zhu P, Balhoff MT. Microfluidic Investigation of Low-Salinity Effects During Oil Recovery: A No-Clay and Time-Dependent Mechanism. SPE J 2019.
[54] Yang L, Zhang X, Zhou T, Lu X, Zhang C, Zhang K. The effects of ion diffusion on imbibition oil recovery in salt-rich shale oil reservoirs. J Geophys Eng 2019;16(3):525–40.
[55] Wen L, Papadopoulos KD. Effects of osmotic pressure on water transport in W1/O/W2 emulsions. J Colloid Interface Sci 2001;235(2):398–404.
[56] Sandengen K, Kristoffersen A, Melhuus K, Jøsang LO. Osmosis as mechanism for low-salinity enhanced oil recovery. SPE J 2016;21(04):1227–35.
[57] Fredriksen SB, Rognmo AU, Fernø MA. Pore-scale mechanisms during low salinity waterflooding: Oil mobilization by diffusion and osmosis. J Petrol Sci Eng 2018;163:650–60.
[58] T. s. E. Chávez-Miyauchi, A. Firoozabadi, and G. G. Fuller, "Nonmonotonic elasticity of the crude oil–brine interface in relation to improved oil recovery," Langmuir, vol. 32, no. 9, pp. 2192-2198, 2016.
[59] Davies J, Wiggill J. Diffusion across the oil/water interface. Proc R Soc Lond A 1960;255(1281):277–91.
[60] Cheng J, Chen J-F, Zhao M, Luo Q, Wen L-X, Papadopoulos KD. Transport of ions through the oil phase of W1/O/W2 double emulsions. J Colloid Interface Sci 2007;305(1):175–82.
[61] Marine IW, Fritz SJ. Osmotic model to explain anomalous hydraulic heads. Water Resour Res 1981;17(1):73–82.
[62] Fritz SJ. Ideality of clay membranes in osmotic processes: a review. Clays Clay Miner 1986;34(2):214–23.
[63] Karadimitriou N, Hassanizadeh S, Joekar-Niasar V, Kleingeld P. Micromodel study of two-phase flow under transient conditions: Quantifying effects of specific interfacial area. Water Resour Res 2014;50(10):8125–40.
[64] Zarikos I, Hassanizadeh S, van Oosterhout L, van Oordt W. Manufacturing a micromodel with integrated fibre optic pressure sensors. Transp Porous Media 2018;122(1):221–34.
[65] Long L, Zhang B. The distribution of fluids in irregular capillary tubes: a new capillary model based on the single-corner capillary. J Pet Explor Prod Technol 2018;8(2):341–50.
[66] H. Suh, D. Kang, J. Jang, K. Kim, and T. Yun, "Capillary pressure at irregularly shaped pore throat," in Proc. of the 7th International Conference on Unsaturated Soils, 2018.
[67] D. Agrawal, K. Xu, Q. Darugar, and V. Khabashesku, "Enhanced Oil Recovery by Nanoparticle-Induced Crude Oil Swelling: Pore-Scale Experiments and Understanding," in SPE Asia Pacific Oil and Gas Conference and Exhibition, 2018: Society of Petroleum Engineers.
[68] E. Unsal and E. Moulet-Vargas, "Impact of wetting film flow in pore scale displacement," in SCA, 2013, vol. 16, p. 2013.
[69] Zheng L, Yapa PD. Modeling gas dissolution in deepwater oil/gas spills. J Mar Syst 2002;31(4):299–309.
[70] Fredriksen S, Rognmo A, Sandengen K, Fernø M. Wettability effects on osmosis as an oil-mobilization mechanism during low-salinity waterflooding. Petrophysics 2017;58(01):28–35.